

# HESS Observations of Pulsar Wind Nebulae

Ocker C. de Jager

*Unit for Space Physics, North-West University, Potchefstroom Campus, Private Bag X6001,  
Potchefstroom, 2520, South Africa*

**Abstract.** The high resolution capabilities of the *High Energy Stereoscopic System (HESS)* introduced a new era in Gamma-Ray Astronomy, and opens a new window on pulsar wind nebula (PWN) research. A rotationally induced jet (associated with PSR B1509-58) is resolved for the first time in  $\gamma$ -rays, allowing us to trace the particle transport directly, without having the complicating effect of spatially varying field distributions on the synchrotron emissivity. For PWN older or more extended than Crab (i.e. those with lower field strengths), *HESS* also reveal the properties of electrons contributing to the EUV/soft X-ray synchrotron bands, whereas EUV/soft X-rays suffer from severe interstellar absorption effects. Finally, *HESS* morphological studies of evolved PWN also allow us to directly measure the effects of asymmetric reverse shock interactions due to SNR forward shock expansion into the inhomogeneous interstellar medium.

**Keywords:** pulsar wind nebulae: general – stars: neutron – gamma-rays

**PACS:** 97.60.Gb

## INTRODUCTION

Weiler & Panagia [1] first coined the term "filled-center" or "plerionic" nebulae, following the discovery of galactic sources with the following features: (1) filled center or blob-like form; (2) a flat radio spectral index between 0 and -0.3; (3) a well organised magnetic field; and (4) a high integrated linear polarisation at high radio frequencies. In 1980, Weiler & Panagia [2] added Vela X, part of the Vela SNR, as a member of this class of sources. The offset of the Vela X PWN relative to the Vela pulsar was puzzling, until resolved as discussed below.

X-ray Astronomy was quite instrumental in detecting and characterising these pulsar wind nebulae (PWN) and we were left with Radio and X-ray Astronomy contributing mostly to our knowledge of PWN, other than the Crab Nebula. A few useful contributions from Infrared Astronomy were also made, filling the spectral gap between radio and X-rays. The radiation mechanism for radio through X-rays is generally believed to be synchrotron emission as a result of pulsar injected electrons, with X-rays resulting from freshly injected electrons, whereas relic electrons contribute mostly to the radio part. The ordered magnetic field is usually toroidal (due to the spinning pulsar), with magnetization resulting from the deceleration of the post-shock pulsar wind flow [3]. The synchrotron brightness is a result of a convolution of the electron density and the magnetic field strength, whereas the same electrons also scatter ambient photons into the high energy to ultra high energy  $\gamma$ -ray range. Both components should be observed to understand the dynamics of the pulsar wind.

The well-known optical "wisps" in the Crab Nebula are believed to mark the pulsar wind shock radius, where the pressure from the unshocked (upstream) pulsar wind

balances the (downstream) nebular pressure [3]. The high resolution X-ray images of *Chandra* contributed significantly to this field, showing that the presence of a torus and perpendicular jet are common to PWN (see [4] and references therein), with an underluminous region on the inner part of the torus, marking the PWN shock radius. Ng & Romani [4] managed to derive the geometry of these structures, which establishes the orientation of the pulsar spin axis (aligned with the X-ray jet) on the plane of the sky. *Thus, unified pulsar-PWN models should combine measured radio pulse polarisation swing data and high resolution X-ray PWN geometry for internal consistency.*

A complicating factor for evolved PWN is the effect of the reverse shock on the PWN for SNR expansion into an inhomogeneous ISM: van der Swaluw et al. [5] showed that after the passage of the reverse shock into the PWN, the latter will expand subsonically, settling to a radius, which is  $\sim 25\%$  of the SNR forward shock radius. Blondin et al. [6] also showed that an inhomogeneous ISM pressure will result in the reverse shock returning to the PWN at different times of its evolutionary history, which can shift the position of the PWN, as observed for Vela X and G 18.0-0.7 (the latter is associated with PSR B1823-13 [7].) *Since most massive star formation is taking place in inhomogeneous molecular clouds, we expect to see several offset PWN, which can be studied with the high resolution imaging capabilities of HESS, since the HESS emitting electron lifetimes can be longer than the epoch of PWN shift.*

A review of the *HESS* telescopes and basic overview of results are given by G. Hermann in these proceedings. In this paper we concentrate on the PWN results of *HESS* and what we learn from these results, combined with multiwavelength information. At the time of the writing of this paper, a number of PWN has been detected by *HESS*, but we only discuss the PWN of SNR G 0.9+0.1, PSR B1509-58, and PSR B 1823-13.

## **HESS J 1747-281 = PWN OF SNR G 0.9+0.1**

Unresolved TeV emission from SNR G 0.9+0.1 was detected after 50 hours of live-time observations [8]. The image in Figure 1a shows that the TeV source is coincident with the PWN, and is smaller than the shell size associated with this composite SNR. This source is one of the weakest TeV sources detected so far, with an integral flux above 200 GeV of  $F(> 200\text{ GeV}) = (5.7 \pm 0.7_{stat} \pm 1.2_{sys}) \times 10^{-12} \text{ cm}^{-2}\text{s}^{-1}$  and a photon spectral index of  $\Gamma_{HESS} = (2.40 \pm 0.11_{stat} \pm 0.20_{sys})$ . This spectrum is shown in Figure 1b [8].

de Jager et al. [9] derived an analytical expression for the TeV  $\gamma$ -ray spectrum in terms of the X-ray spectrum, assuming that the X-ray spectrum with energy index  $\alpha_x$  (between 0 and 2.5) extends to the EUV/soft X-ray range, since synchrotron emitting electrons producing such soft emission also IC scatter CMBR photons into the TeV range for a magnetic field strength in the range  $\sim 10\mu\text{G}$ . The IC  $\gamma$ -ray energy spectrum (with  $E_{\text{TeV}}$  the  $\gamma$ -ray energy in units of TeV) at earth, written in terms of the observed monochromatic X-ray flux  $S_{1\text{keV}}$  at 1 keV is then (in units of  $\text{TeV}/\text{cm}^2/\text{s}/\text{TeV}$ )

$$S_{2.7\text{K}}(E_{\text{TeV}}) = 6.6 \times 10^{-17} \frac{(1.4 \times 10^{-5})^{\alpha_x}}{B_{\perp}^{(\alpha_x+1)}} \exp [2.2\alpha_x - 0.126\alpha_x^2] S_{1\text{keV}} C_{2.7\text{K}} E_{\text{TeV}}^{-\alpha_x},$$

with the first-order Klein-Nishina correction function given by  $C_{2.7\text{K}} = [1 - (2.4 +$

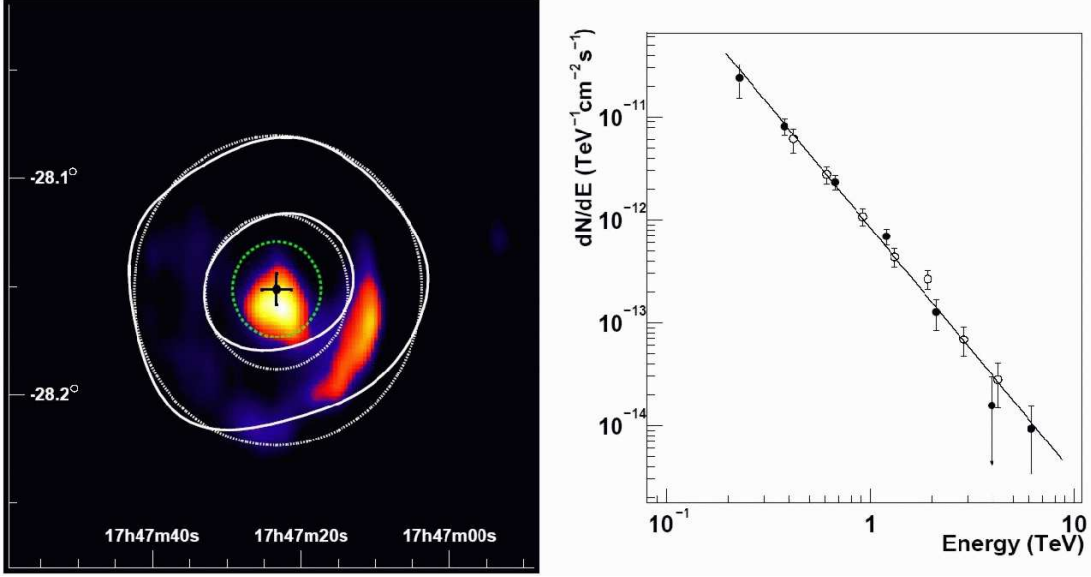


**FIGURE 1.** (a) Left: The 90 cm radio flux map of G0.9+0.1 with HESS confidence contours: white solid (dashed) circles: observed (simulated point spread function) 40% and 80% peak brightness; green dashed circle: 95% upper limit on *HESS* source size. (b) Right: The *HESS* photon spectrum of G0.9+0.1.

$3.9\alpha_x + 0.42\alpha_x^2(0.03E_{\text{TeV}})^{1/2}$ ]. If IC emission on the 25K galactic (or swept-up) dust component (with density  $U_{25}$  in units of  $\text{eV}/\text{cm}^3$ ) is important, we have to add the additional IC TeV flux given by the expression:

$$S_{25\text{K}}(E_{\text{TeV}}) = 0.023(25/2.7)^{\alpha_x}(\alpha_x + 3)(\alpha_x + 4)U_{25} \left[ \frac{S_{2.7\text{K}}(E_{\text{TeV}})}{C_{2.7\text{K}}} \right] C_{25\text{K}},$$

with the first-order Klein-Nishina correction now larger [9]  $C_{25\text{K}} = [1 - (2.4 + 3.9\alpha_x + 0.42\alpha_x^2)(0.09E_{\text{TeV}})^{1/2}]$ . This correction function is only valid for  $C < 0.5$  and higher order corrections are then necessary for larger energies.

Milky Way type galaxies show that the IR emission from dust dominates the starlight component near the galactic center (R. Tuffs & C. Popescu, personal communication, 2005), contrary to the assumption in [8], where the starlight was assumed to dominate the dust component. This observation also makes the interpretation of the TeV spectrum simpler as discussed below:

*XMM Newton* observations of G0.9+0.1 showed that the energy index  $\alpha_x = \Gamma_X - 1$  increases with increasing radius (possibly due to synchrotron cooling), giving a value of  $\alpha_x = 1.4 \pm 0.2$  for an outer shell of radius 1.8 to 3.5 pc [10], which is larger compared to the 0.6 pc size of the Crab X-ray nebula. It is reasonable to assume that the field strength in this outer region would be smaller compared to the compact core, so that most electrons have accumulated here over the pulsar lifetime, resulting in the observed IC TeV emission. The 95% upper limit on the *HESS* source radius (containing 68% of the events) is also 3.2 pc [8] (assuming a distance of 8.5 kpc to the galactic center.) The *HESS* source therefore includes the total X-ray PWN and we expect most *HESS* emitting electrons to be concentrated in the region where the field is lowest and volume is largest.

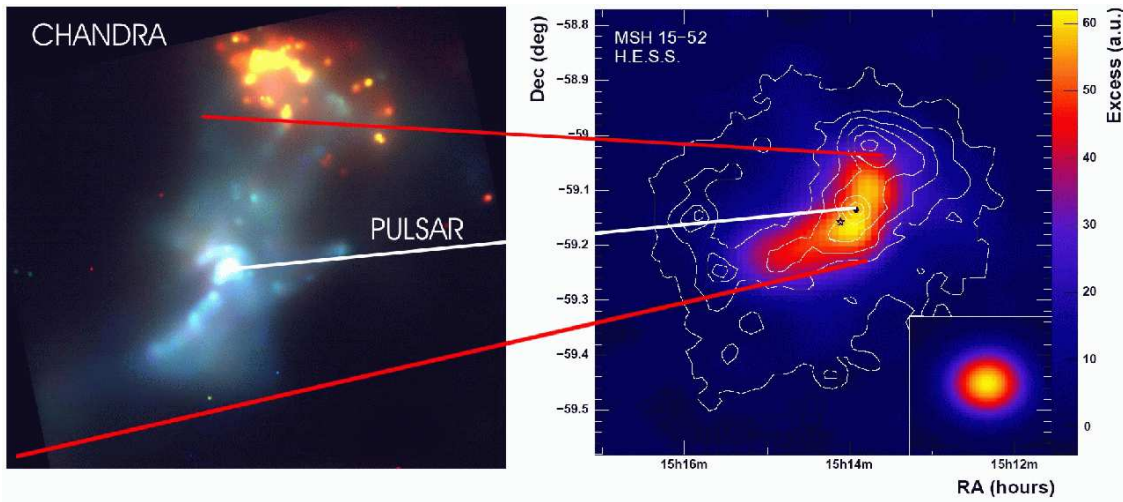


**FIGURE 2.** (a) Left: The *Chandra* image of the PWN of PSR B1509-58, indicated by the extended blue jet and compact torus perpendicular to the jet, centered on the pulsar. The red structure at the top is the thermal nebula RCW 89, undetected by *HESS* [13]. (b) Right: The *HESS* image of the PWN of PSR B1509-58, showing a similar jet structure as indicated by the projection from *Chandra* (red and white lines) and the *ROSAT* PSPC contour overlay (white contours) [12].

It also appears to be valid to extrapolate the X-ray spectrum into the EUV range, since the spectral break between radio and X-rays is only observed around  $10^{11}$  to  $10^{12}$  Hz [11]. The photon index of TeV emission should therefore also be  $\Gamma_{HESS} \sim a_x + 1 = 2.4$  (as observed.) Assuming a monochromatic flux of  $S_{1\text{keV}} = 0.0014 \text{ cm}^2/\text{s}/\text{keV}$  at 1 KeV [10], we calculate a magnetic field strength in the large outer volume of the PWN as  $10\mu\text{G}$ , assuming a 25K photon density of  $1 \text{ eV}/\text{cm}^3$  in this region of the galaxy. However, a 2.3 times higher density would give a field strength of  $\sim 14\mu\text{G}$ .

*Thus, the agreement between the X-ray and TeV spectral indices (within uncertainties) exclude the need to invoke a dominant central starlight component, consistent with observations of other Milky Way type galaxies.* Furthermore, a more detailed MHD approach is needed to put constraints on the injection parameters of the unseen pulsar.

## HESS J1514-591 = PWN OF PSR B1509-58

This source was easily detected by *HESS*, with a significance of  $25\sigma$  after 22 hours of observation [12]. Good statistics allowed the measurement of the TeV spectrum with high precision: The monochromatic flux at 1 TeV is  $(5.7 \pm 0.2_{\text{stat}} \pm 1.4_{\text{sys}}) \times 10^{-12} \text{ cm}^{-2}\text{s}^{-1}\text{TeV}^{-1}$ , and the power law spectral index is  $\Gamma_{HESS} = (2.27 \pm 0.03_{\text{stat}} \pm 0.20_{\text{sys}})$  for the range 0.28 to 40 TeV. The power law is unbroken [12].

From Figure 2 we see that the TeV morphology follows the X-ray morphology in terms of the jet-like structure: This pulsar also shows a torus and jet, with the torus clearly resolved by *Chandra* [13]. Contrary to other compact PWN, the jet dominates the toroidal component, and the same is seen in TeV  $\gamma$ -rays. *This is the first time that an astrophysical jet has been resolved in the  $\gamma$ -ray domain.* The TeV emission extends to a

radius of  $0.3^\circ$  (or 25 pc) from the pulsar, assuming a distance of 5 kpc to the pulsar

Whereas the jet close to the pulsar reveals a photon index of  $\Gamma_{\text{cn}} = 1.6 \pm 0.1$  (with "cn"="compact nebula" derived from feature "C" of [13]), the diffuse emission up to  $0.3$  degrees reveal a spectral index of  $\Gamma_{\text{en}} = 2.04 \pm 0.01$  ("en"="extended nebula", [14]). This steepening (by  $\Gamma_{\text{en}} - \Gamma_{\text{cn}} = 0.44 \pm 0.10$ ) is consistent with synchrotron cooling. The TeV emission corresponds to this extended cooled region and the additional steepening  $\Gamma_{\text{HESS}} - \Gamma_{\text{en}} = 2.27 - 2.04 = 0.23$  can be explained by the addition of a 25K dust component by galactic and swept-up dust in the SNR of this pulsar [15, 12]. A discussion of the cooling break will be given below.

Aharonian et al. [12] found that galactic dust emission at a level of  $2.3 \text{ eV/cm}^3$  could explain the observed *HESS* spectrum, assuming a mean magnetic field strength of  $17 \mu\text{G}$  in this extended region. Before the *HESS* era, Gaensler et al. [13] argued that the spectral break due to synchrotron losses should be just below 1 keV (for an  $8 \mu\text{G}$  field), whereas the field strength of  $17 \mu\text{G}$  derived from TeV observations predicts a spectral break near 3 TeV, which is not observed [12]. Note however that this cooling break scales as  $B^{-4}T^{-2}$  in the Thomson limit, and that the nebular field strength was larger during earlier epochs (i.e. expansion causes the field strength to decrease with time). Just a factor two larger  $B$  (without changing the spindown age), during earlier epochs, will already push the spectral break down by a factor of 16. The result is then an unbroken power law down to at least 0.3 TeV, as observed. *Thus, more realistic PWN models should allow for field evolution with time, whereas constant field models may predict a TeV spectral break, which is not observed.*

### **HESS J1825-137 = (?) G 18.0-0.7 = PWN OF PSR B1823-13**

The source HESS J1825-137 was discovered as part of the *HESS* galactic plane survey [16]. It is resolved with an RMS radius of  $\sim 10'$ , and the 101 ms period Vela-like pulsar, PSR B1823-13, is the only candidate source within the area resolved by *HESS*. The *HESS* Collaboration recently made a case for the association of HESS J1825-137 with G 18.0-0.7, based on morphological and spectral considerations [17].

Despite the fact that the X-ray PWN G 18.0-0.9 is located south of this 21 kyr old pulsar, the association between the pulsar and the X-ray PWN is considered to be firm [7]. Figure 3a shows an excess slice plot taken along the north-south direction, showing this asymmetry. Gaensler et al. [7] invoked the Vela X type explanation of Blondin et al. [6] to explain the southwards offset of the PWN relative to PSR B1823-13. From Figure 3a we can see that the bright X-ray compact nebula (containing freshly injected, uncooled electrons) is symmetric with respect to the pulsar, whereas the older (cooled) electrons result in a southward offset X-ray nebula. The TeV nebula is also shifted to the south (Figure 3b), with an extension ( $\sim 0.5^\circ$ ), which is even larger compared to X-rays. This is expected based on the longer synchrotron lifetimes of TeV vs X-ray emitting electrons.

The  $0.5^\circ$  diameter of the TeV source translates to a radius of  $R_{\text{PWN}} \sim 17d_4$  pc for a distance of  $d = 4$  kpc. The SNR forward shock radius is then expected to be  $R_{\text{SNR}} \sim 4R_{\text{PWN}} = 70d_4$  pc [5], which can be reached if we invoke a relatively large initial spindown power and pulsar braking index less than the canonical value of  $n = 3$ ,

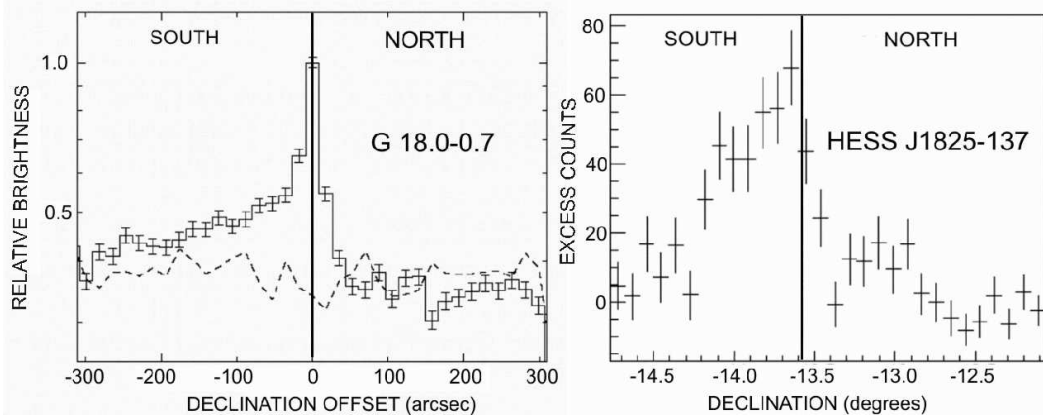


**FIGURE 3.** (a) Left: The *XMM* north-south excess slice of the PWN of PSR B1823-13 (from [7]), (b) Right: similar north-south slice of HESS J1825-137, also showing emission south of the pulsar, but over a much larger size (from [17].)

to increase the age of the SNR. The Sedov-Taylor SNR size would also increase with increasing age, giving a radius of

$$R_{SNR} = 78 \text{pc} \left( \frac{E_{SN}}{10^{51} \text{ergs}} \frac{0.003 \text{cm}^{-3}}{N} \right)^{0.2} \left( \frac{1}{n-1} \right)^{0.4}.$$

Here  $E_{SN} \sim 10^{51}$  ergs is the SN explosion energy and  $N \sim 0.003 \text{cm}^{-3}$  is the density of the hot phase of the ISM. A pulsar braking index of  $n = 2$  (“LMC pulsar” type) will then increase the age of PSR B1823-13 to  $\sim 42$  kyr, which would imply a size consistent with the predicted size of the unseen SNR shell of  $\sim 70$  pc.

## REFERENCES

1. K. W. Weiler, and N. Panagia, *Astron. Astrophys.*, **70**, 419 (1978).
2. K. W. Weiler, and N. Panagia, *Astron. Astrophys.*, **90**, 269–282 (1980).
3. C. F. Kennel, and F. V. Coroniti, *Astrophys. J.*, **283**, 710–730 (1984).
4. C.-Y. Ng, and R. W. Romani, *Astrophys. J.*, **601**, 479–484 (2004).
5. E. van der Swaluw, *et al.*, *Astron. Astrophys.*, **380**, 309–317 (2001).
6. J. M. Blondin, R. A. Chevalier, and D. M. Frierson, *Astrophys. J.*, **563**, 806–815 (2001).
7. B. M. Gaensler, N. S. Schulz, V. M. Kaspi, M. J. Pivovarov, and W. E. Becker, *Astrophys. J.*, **588**, 441–451 (2003).
8. F. Aharonian, and *HESS* Collaboration, *Astron. Astrophys.*, **432**, L25–L29 (2005).
9. O. C. de Jager, *et al.*, *Proc. 24th Int. Cosmic Ray Conf.*, **4**, 528–531 (1995).
10. D. Porquet, A. Decourchelle, and R. S. Warwick, *Astron. Astrophys.*, **401**, 197–203 (2003).
11. L. Sidoli, *et al.*, *Astron. Astrophys.*, **361**, 719–724 (2000).
12. F. Aharonian, and *HESS* Collaboration, *Astron. Astrophys.*, **435**, L17–L20 (2005).
13. B. M. Gaensler, *et al.*, *Astrophys. J.*, **569**, 878–893 (2002).
14. T. Mineo, *et al.*, *Astron. Astrophys.*, **380**, 695–703 (2001).
15. I. Du Plessis, *et al.*, *Astrophys. J.*, **453**, 746 (1995).
16. F. Aharonian, and *HESS* Collaboration, *Science*, **307**, 1938–1942 (2005).
17. F. Aharonian, and *HESS* Collaboration, *Astron. Astrophys.*, p. Accepted for publication (2005).